© 2014. Published by The Company of Biologists Ltd | The Journal of Experimental Biology (2014) 217, 3263-3273 doi:10.1242/jeb.108076

RESEARCH ARTICLE

Hiding opaque eyes in transparent organisms: a potential role for larval eyeshine in stomatopod crustaceans

K. D. Feller* and T. W. Cronin

ABSTRACT

Opaque screening pigments are a fundamental requisite for preserving resolution in image-forming eyes. Possession of any type of image-forming eye in a transparent, pelagic animal will thus undermine the ability of that animal to be invisible in the water column. Transparent, pelagic animals must therefore deal with the trade-off between the ability to see and the ability of other animals to see them. Stomatopod larvae, like many transparent crustaceans, possess specialized optics in their compound eyes that minimize the volume of the opaque retina. Though the volumes of these retinas are reduced, their opacity remains conspicuous to an observer. The light reflected from structures overlying the retinas of stomatopod crustacean larval eyes, referred to here as eyeshine, is hypothesized to further reduce the visibility of opaque retinas. Blue or green wavelengths of light are most strongly reflected in stomatopod larval eyeshine, suggesting a putative spectral matching to the light environment against which the larval eyes are viewed. We tested the efficacy of stomatopod crustacean larval eyeshine as an ocular camouflaging mechanism by photographing larvae in their natural light environment and analysing the contrast of eyes with the background light. To test for spectral matching between stomatopod larval eyeshine and the background light environment, we characterized the spectrum of eyeshine and calculated its performance using radiometric measurements collected at the time of each photographic series. These results are the first to demonstrate an operative mirror camouflage matched in both spectrum and radiance to the pelagic background light environment.

KEY WORDS: Camouflage, Larva, Stomatopod, Visual ecology

INTRODUCTION

For small animals in the pelagic environment, such as marine crustacean larvae, survival in such a featureless world often depends on the ability to avoid being seen. Given this strong selection for crypsis, multiple mechanisms have evolved in open-water habitats that facilitate the visual melding of an animal's body into its surroundings, the most notable being mirrored sides (Denton et al., 1972; Johnsen and Sosik, 2003), counterillumination (Clarke, 1963; Johnsen et al., 2004), and transparent body tissue [reviews of transparency (Breder, 1962; McFall-Ngai, 1990; Johnsen, 2001); reviews of general pelagic camouflaging mechanisms (Nilsson, 1995; Johnsen, 2014)]. Many crustacean larvae provide exquisite examples of the latter mechanism, possessing bodies that are so transparent they are seemingly made of glass. The compound eyes are the only features containing opaque pigments in these animals. Though crustacean larval eyes have evolved to increase their transparency with elongated optical elements and condensed retinas (Nilsson, 1983), opaque screening pigments must remain between photoreceptors in order to preserve resolution of the visual scene. Among crustacean larvae, the stomatopods are particularly effective at maximizing their transparency. Often, the eyes are the only visible features on a stomatopod larval body, which depending on the species, can be up to 40 mm long (Feller et al., 2013). Thus to a human peering into a bucket of plankton, stomatopod larvae may only appear as moving pairs of black dots fixed side-by-side as the animal pirouettes through space.

Undescribed structures within stomatopod larval eyes strongly reflect blue or green wavelengths of light, referred to here as eyeshine (Fig. 1). The eyeshine discussed here is not to be confused with that produced by the light-reflecting tapetum observed beneath the rhabdoms of some crustacean eyes (such as those of *Nephrops norvegicus*) (Loew, 1976). Careful observation of the reflecting material responsible for stomatopod larval eyeshine suggests that it includes a photonic structure found between the optical and photoreceptor layers of the eye, but absent from the optical pathway (Fig. 1C). The absence of eyeshine from the pathway of light absorbed by photoreceptors (as evidenced by the presence of a robust pseudopupil) suggests that eyeshine does not function as a visual filtering mechanism or otherwise act to influence photoreception in these eyes. We have observed stomatopod eyeshine in all stomatopod larval eyes examined to date, regardless of species or stage (authors' personal observation) (see also Williams et al., 1985; Cronin et al., 1995; Jutte et al., 1998; Cronin and Jinks, 2001). Outside of stomatopod larvae, the presence of eyeshine has been observed in brachyuran crab larvae (authors' personal observation) (Cronin and Jinks, 2001), embryonic and larval caridean shrimp [*Palaemonetes pugio* (Douglass and Forward, 1989); *P. argentinus* (Harzsch et al., 1999)], embryos of the American lobster [*Homarus americanus* (Harzsch et al., 1998)], and the adult isopod *Astacilla longicornis* (Nilsson and Nilsson, 1983). With no apparent role in photosensitivity, eyeshine is instead hypothesized to serve as a pelagic camouflage for the conspicuous retina over which it is produced (Nilsson and Nilsson, 1983; Douglass and Forward, 1989; Cronin et al., 1995; Jutte et al., 1998; Cronin and Jinks, 2001). Though the role of crustacean larval eyeshine has been posited as a camouflage many times, the hypothesis has never been formally tested. We sought to test the eyeshine camouflage hypothesis by analysing several components of eyeshine in the natural viewing environment of stomatopod larvae. Through imaging and analysis of spectral reflectance of stomatopod larval eyeshine both in the laboratory and in the natural light environment, we tested the efficacy of eyeshine at reducing the inherent contrast of the larval retina at different depths, orientations and periods of the day. These data provide sound support for the hypothesis that stomatopod larval eyeshine functions as an ocular camouflaging mechanism.

University of Maryland Baltimore County, 1000 Hilltop Circle, Baltimore, MD 21250, USA.

*Author for correspondence (kfeller1@umbc.edu)

Received 15 May 2014; Accepted 23 June 2014

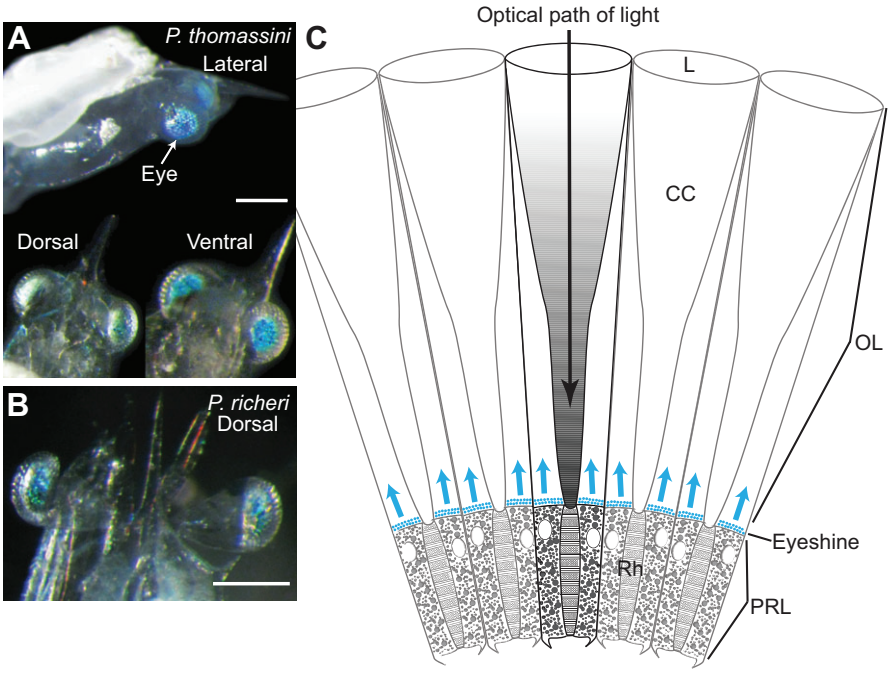

Fig. 1. Stomatopod larval eyeshine. Photographs of (A) *Pullosquilla thomassini* and (B) *Pseudosquillana richeri* individuals used in these experiments. Lateral, dorsal and ventral images of *P. thomassini* in A show the change in eyeshine brightness and color across the eye, a characteristic of this species. (C) Diagram depicting the putative location of photonic structures responsible for producing stomatopod larval eyeshine. PRL, photoreceptor layer; Rh, rhabdom; L, lens; CC, crystalline cones; OL, optical layer. Scale bars, 500 μm.

RESULTS

Post hoc animal identification

Three species of stomatopod larvae were sampled in this study, representing three of the seven superfamilies presently described in Stomatopoda: *Pullosquilla thomassini* Manning (*N*=6; Lysiosquilloidea), *Pseudosquillana richeri* Moosa (*N*=1; Pseudosquilloidea), and an unknown species of *Harpiosquilla* (*N*=1; Squilloidea). Each sampled individual was an early stage larva that did not molt between nocturnal capture and daytime imaging. We could not assign individuals to a specific developmental stage since there are no published descriptions of the larval stages available for either of the identified species. It can be inferred, however, that given the similarities in size and morphology, the six sampled *P. thomassini* individuals were most likely the same developmental stage.

Image contrast analysis

Animals were photographed under water, in their natural environment at a variety of positions, depths, and illumination conditions selected to most broadly sample views of an animal in the upper hemisphere of three-dimensional space from a fixed observer on the benthos (Fig. 2, see '*In situ* imaging' in Materials and methods). Within each photograph a small, opaque dark standard and/or a dead animal with degraded eyeshine was also imaged as a control. From each of these photographs, Michelson contrast values were calculated between the larval eyespot (or control) and the background. Michelson contrast is a metric that contains information regarding the relative brightness or darkness of an object against a background. Per the definition of Michelson contrast (see Materials and methods), values range between −1 and 1 with a value of zero equal to no contrast.

All Michelson contrast values of larval eyeshine with the background light environment are reasonably close to 0.0 (value of no contrast). These results are consistent among the three species measured and at all depths, azimuth directions, elevation angles, rotations, and refracted solar elevations (Fig. 3). Data in Fig. 3 are presented using a gray scale to visually represent individual contrast values from each azimuth angle, viewing angle above the horizon, axial orientation, and rotation measured from four individuals that represent all studied species and depths, as well as the corresponding dark standard (depicted in Fig. 2).

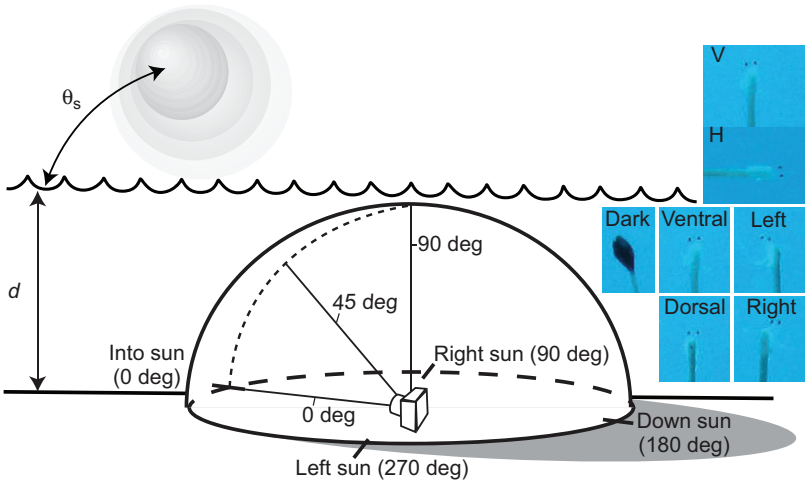

Fig. 2. *In situ* imaging and radiometric experimental design. Depicted here are all directional variables included for underwater photographic and environmental radiometric data collection. Data were collected at different depths (*d*) and at different times of day or solar elevations (θ_s). Photographs and radiometric probe directions were oriented in four directions relative to the sun (Into sun 0 deg, Right sun 90 deg, Down sun 180 deg, Left sun 270 deg). At each sun direction, measurements were made with the animal positioned with its body axis horizontal (H) or vertical (V) in three angles relative to the horizon (0, 45 and 90 deg). At each position in space, each animal was rotated in four positions (Ventral, Left, Dorsal and Right). Inset photographs depict these four rotational positions, the dark standard (Dark), and H versus V body axes.

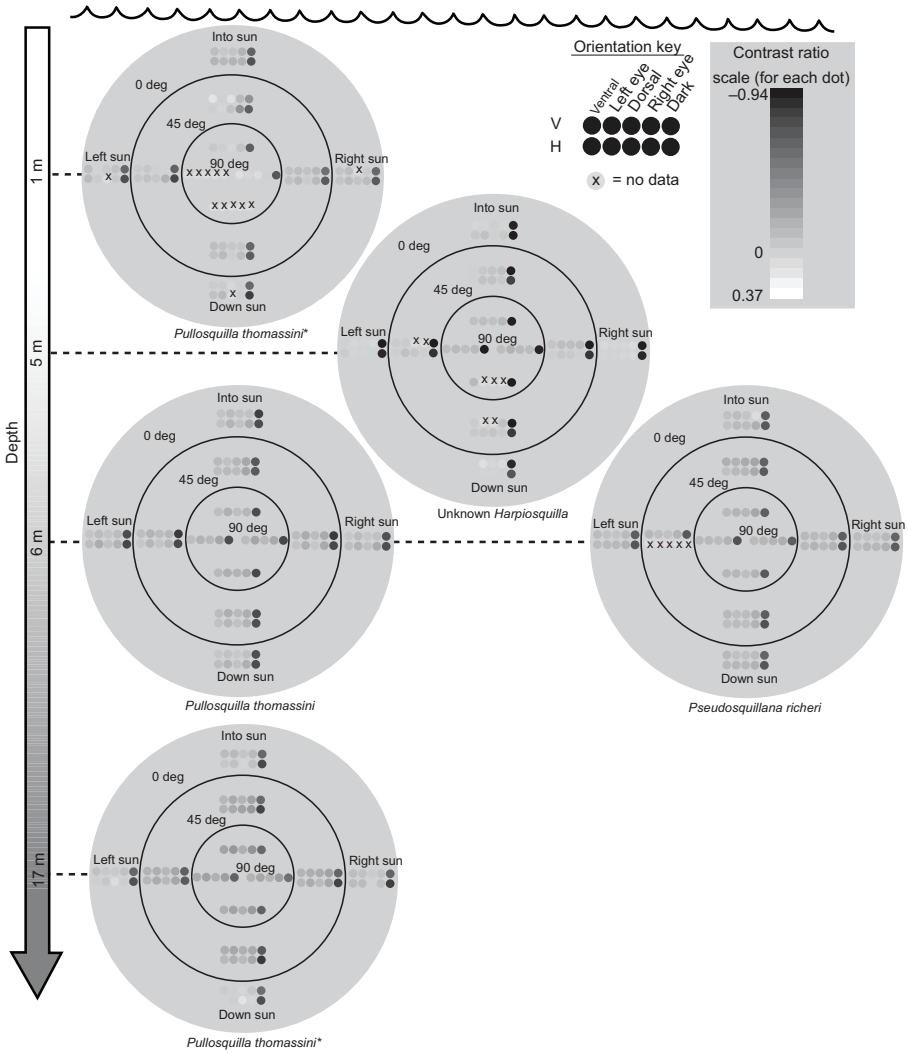

Fig. 3. *In situ* contrast values from stomatopod larvae. Each circle plot represents data from an individual of a given species at the indicated depth (dotted line). Dots within each plot represent the average Michelson contrast value of three different exposures taken at each animal rotation (Ventral, Left eye, Dorsal, Right eye), axis orientation (H, horizontal; V, vertical), viewing angle to the horizon (0, 45, 90 deg), and solar azimuth direction (Into sun, Right sun, Down sun, Left sun). The last dot of each set represents the contrast values measured from the dark standard. Due to redundancy of images between H and V axis orientations at the 90 deg overhead viewing angle, only the H series of data were collected for each solar azimuth direction, which produced only four data points per solar azimuth direction at this viewing angle. Dots are shaded in a scale from black to white that correspond to the range of Michelson contrast values from negative to positive, respectively (see inset contrast ratio scale). Dots representing values of no contrast, 0.0, are shaded the same as the background and thus appear to be missing at these positions Dots with an 'X' denote points where contrast values could not be extracted from the sample photograph. * Indicates the same individual at two different depths.

Data points, or dots, in Fig. 3 are shaded such that the contrast value of 0.0 (the value of no contrast) equals the gray circular background and contrast values above or below 0.0 are lighter or darker gray, respectively. Thus the closer a value of contrast is to 0.0 at a given viewing co-ordinate, the less discernable the dot is on the plot.

Table 1. Results from pair-wise statistical analyses of Michelson contrast data sets

Test	Contrast data set	*N*	Mean	Median	s.d.	α	*P*
Wilcoxon rank-sum	All (8) larval individuals	803	−0.09	−0.09	0.07	0.025	<0.001
	All dark standards	205	−0.6	−0.61	0.12		
	All dead eyes	128	−0.25	−0.24	0.08	0.025	<0.001
	All *Pu th6*	150	−0.11	−0.11	0.05		
	Pu th4 (17 m)		−0.25	−0.24	0.08	0.025	<0.001
	Pu th2 (17 m)		−0.11	−0.11	0.05		
Wilcoxon signed rank	*Pu th1*						
	1 m/47 deg	55	−0.075	−0.072	0.05	0.025	0.0025
	11 m/61 deg	55	−0.0098	−0.013	0.14		
	Pu th2						
	1.5 m/52 deg	69	−0.05	−0.06	0.05	0.017	<0.001
	17 m/60 deg	69	−0.12	−0.13	0.08		
	Pu th6						
	6 m/49 deg	76	−0.099	−0.096	0.06	0.017	0.029 n.s.
	6 m/80 deg	74	−0.11	−0.11	0.04		

Different data set comparisons visualized in Fig. 4. Depth and solar elevation information given as data set identifiers for paired data from a single individual. *N*, number of contrast values in data set; s.d., standard deviation; α, significance threshold after Bonferroni correction; *P*, probability value; n.s., not significant. Uncorrected significance threshold was 0.05.

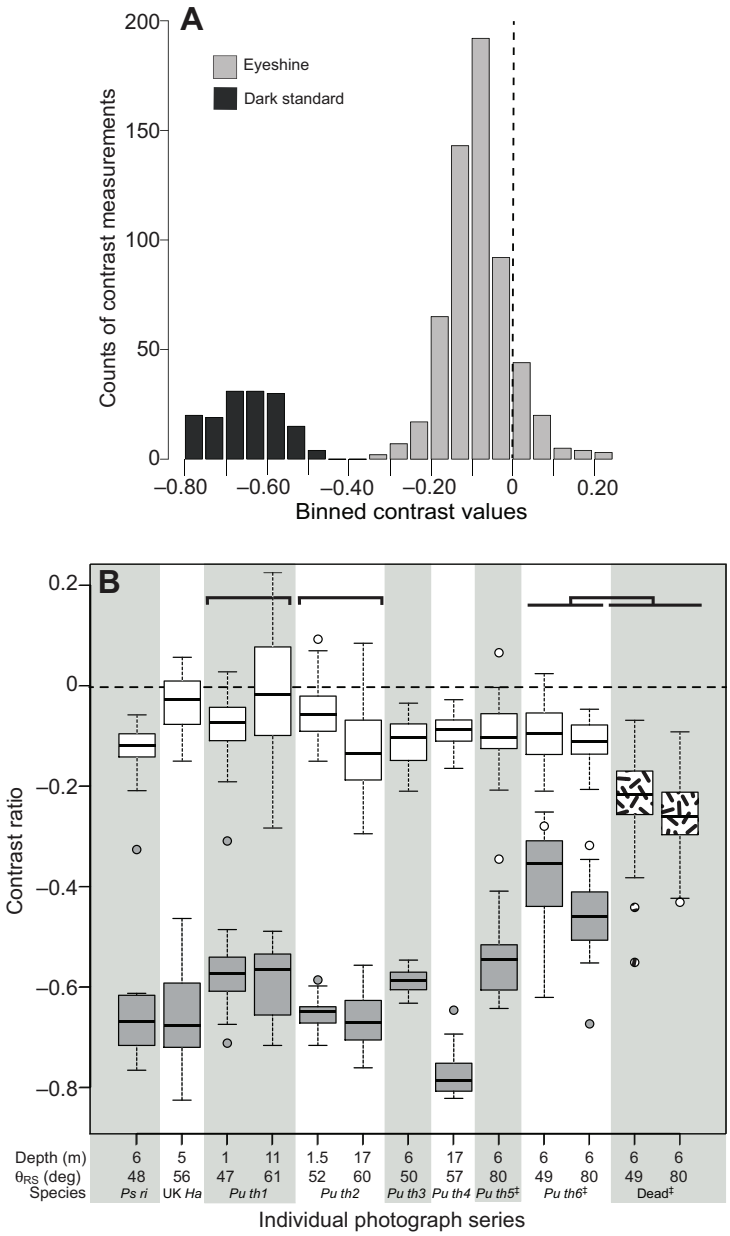

Fig. 4. Summary of image contrast analysis. (A) Histogram of binned contrast values (bin size, 10 deg) from all sampled individuals (gray shading; includes: *P. thomassini*, *N*=4; *P. richeri*, *N*=1; unknown *Harpiosquilla*, *N*=1) and dark standards (black shading). Each contrast value represents the average of three raw contrast values measured at different image exposures for a given orientation or rotation angle in space. Since dark standards were only measured for axis orientation, solar azimuth and horizontal elevation directions (not for animal rotations), the dark standard data set contains one-quarter as many values as the eyeshine data. Dark standard contrast values were significantly different from those of eyeshine (Table 1). (B) Box plots of all measured eyeshine and control contrast values by individual photographic series. Box, interquartile range; whiskers, 1.5 interquartile range; circular dots, outliers. Median is denoted by a continuous, black horizontal line in each box. Boxes and outliers are shaded as follows: white, live animal eyeshine contrast; solid gray, dark standard contrast; stippled, dead eye contrast. Note that some experimental outliers overlap with dark standard data. Gray and white vertical bars in background visually separate box plots by individual photographic series. Three individuals (*Pu th1*, *Pu th2* and *Pu th6*) were imaged twice under different illumination conditions (different depths or θ_{RS}). Brackets at the top of the box plot indicate data sets included in separate pair-wise statistical tests summarized in Table 1. *Pu th*, *Pullosquilla thomassini* (individuals 1−6); *Ps ri*, *Pseudosquillana richeri*; *UK Ha*, unknown *Harpiosquilla*; Dead, dead eye animal control (likely *P. thomassini*) imaged with *Pu th6.* Dashed line represents 0.0 value of no contrast with the natural environment. θ_{RS}, refracted solar elevation of the sun. ‡March 2014 samples. Number of contrast values represented in the box plot of each data set are as follows: *Ps ri*, 76; *UK Ha*, 73; *Pu th1* 47 deg, 58; *Pu th1* 61 deg, 77; *Pu th2* 52 deg, 69; *Pu th2* 60 deg, 80; *Pu th3*, 80; *Pu th4*, 80; *Pu th5*, 60; *Pu th6* 49 deg, 76; *Pu th6* 80 deg, 74; Dead 49 deg, 65; Dead 80 deg, 63.

Overall, 95% of total eyeshine contrast values occurred within a range of −0.346 to 0.225 (Table 1, Fig. 4). All eyeshine contrast values measured from eight individuals were significantly different from those of all dark standards (Table 1, Fig. 4A). There was also a significant difference between the contrast values of the living individual (*Pu th6*) and the contrast values of the dead eye control with which it was imaged at different solar elevations (Table 1, Fig. 4B).

Though all eyeshine contrast values fall near 0.0, there are differences in the variation of eyeshine contrast related primarily to two of the measured variables: solar elevation and depth. Sequential photographic series of the same individual imaged at two different depths and solar elevations produced different ranges, or variations in contrast values (observed in both *Pu th1* and *Pu th2*). The variation in contrast values in the first photographic series [deep depth 11−17 m, refracted solar elevation of the sun (θ_{RS}) 60−61 deg] was significantly different from the second series (shallow depth 1−1.5 m, θ_{RS} 47−52 deg) for each of these individuals (Table 1, Fig. 4B). Unfortunately, the contributions of depth and/or solar elevation to variations in contrast were unable to be deciphered definitively.

In a separate set of imaging experiments performed in March 2014, *P. thomassini* individual 6 (*Pu th6*) was photographed at the same depth (6 m) and location at different times of day (θ_{RS} 49 and 80 deg). This experiment specifically tested the effects of solar elevation on contrast performance at a given depth. The difference in contrast values between the two solar elevations was not significant after Bonferroni correction (Table 1).

Spectral properties of larval eyeshine

Prior to analysing the inherent contrast of larval eyeshine in the natural environment, we characterized some of the fundamental properties of stomatopod larval eyeshine reflectance in an independent set of experiments conducted in June 2010 (Fig. 5). These data provide a general characterization of how eyeshine varies with angle of illumination and polarization in *P. thomassini* and *Gonodactylaceus falcatus*. Though *G. falcatus* was not sampled during our contrast analysis experiments, these data (collected June

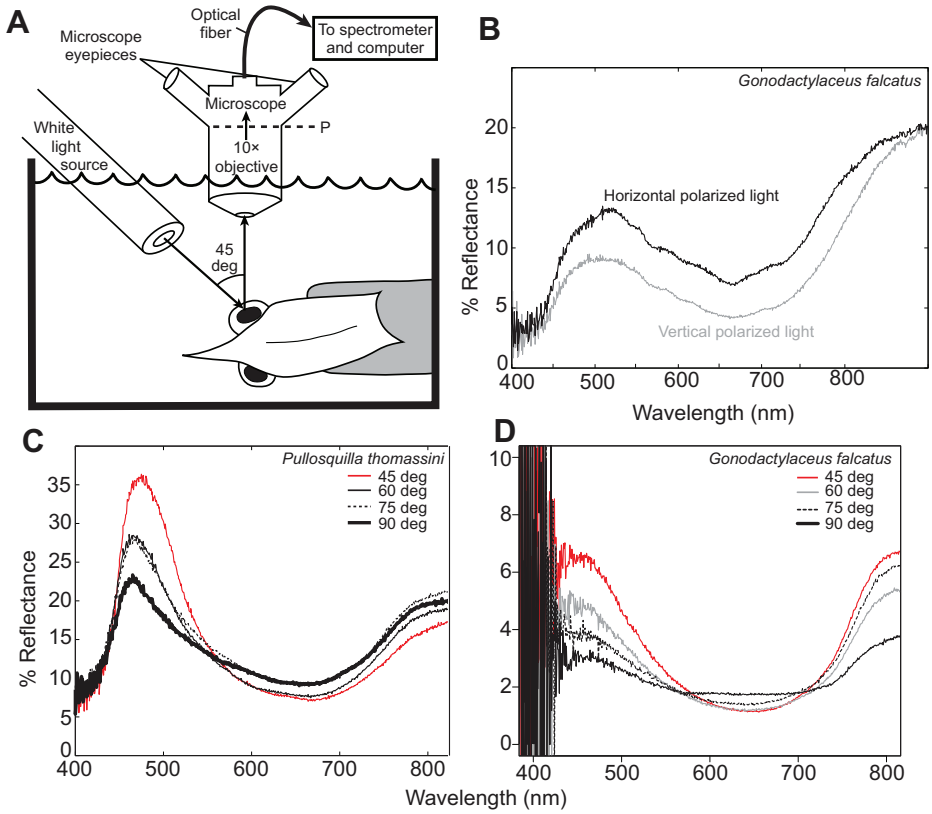

Fig. 5. Characterization of stomatopod larval eyeshine reflectance. (A) Diagram of experimental set-up for measurement of eyeshine reflectance (not drawn to scale). Larvae were fixed to a thin plastic rod and illuminated by a submerged white light source fixed at 45 deg to a submerged 10× objective in seawater. The illuminated larval eye was imaged through a microscope, and the reflectance was measured via a spectrometer and computer system attached to the trinocular head via a 1000 μm optical fiber. For polarization measurements, linear polarizers were placed at location of dashed line, P. (B) Horizontal (0 deg) and vertical (90 deg) e-vector polarization reflectance measurements of eyeshine reflectance in *G. mutatus* from 45 deg illumination. (C) Larval eyeshine reflectance from different illumination angles relative to the 10× objective axis measured from *Pullosquilla thomassini* and (D) *Gonodactylaceus mutatus*. The low levels of short-wavelength light available from the light source combined with the relatively weak reflectance of the eye (due to eye area) is responsible for the noise observed below 410 nm in D.

2010) provide a fundamental understanding of the spectral properties of larval eyeshine necessary for further analyses among a wider range of species.

Most eyeshine reflectance spectra, regardless of species, contain two characteristic peaks in reflectivity: a short-wavelength peak (450–550 nm) and a long-wavelength peak (>800 nm; Fig. 5B–D). In order to resolve the contribution of eyeshine to the observed reflectance spectra, we chose to examine the linear polarization properties of stomatopod larval eyeshine reflectance. It is well established that reflective structures often produce spectra that are linearly polarized (Chiou et al., 2007; Douglas et al., 2007; Stavenga et al., 2010; Stavenga et al., 2011); thus we expected only the portions of the reflectance curve contributed by eyeshine structures to respond to polarization filtering. We observed strong changes in polarization in the short-wavelength region of the reflectance curve, which suggests that eyeshine-producing structures most strongly reflect in this region of the reflectance spectrum (*G. falcatus* data in Fig. 5B). The second, long-wavelength peak in an eyeshine reflectance curve is weakly polarized at most (Fig. 5B), suggesting that it arises from ommochrome screening pigments expressed in the opaque portion of the retina (Marshall et al., 1991).

The amount of light reflected from eyeshine is strongly associated with the stage, and thus eye-size of the animal. The eye diameter of an early stage larva in species such as *P. thomassini* and *G. falcatus* is ~500 μm. A last stage larva of either of these species will have a retinal area that is roughly twice that and thus reflect more light to the spectrometer. With the exception of the last stage *P. thomassini* individual measured in Fig. 5C, all eyeshine reflectances presented are from early stage larvae. The low levels of light reflected from small, early stage eyes results in the spectral noise observed at wavelengths below 410 nm in Fig. 5D and Figs 6–8. It should be noted that while the amount of light reflected changes with ontogeny of the eye, the spectral shape of eyeshine reflectance remains constant across developmental stages.

To determine the illumination angle that would produce the maximum eyeshine reflectance, we measured eyeshine reflectance from four illumination angles (45, 60, 75 and 90 deg relative to the 10× objective). Maximum eyeshine reflectance was measured at an illumination angle of 45 deg of a dorsal-laterally positioned eye, which was also the minimum illumination angle possible within our apparatus (Fig. 5C,D).

Pullosquilla thomassini eyeshine is unlike that of other examined stomatopod larval species, both examined in this study and among all crustacean larval species examined to date (K. D. Feller, unpublished data and personal observations). In both early and late stage larvae, the ventral region of each eye appears blue, and the color transitions to green as one travels across the retina to the dorsal eye region (Fig. 1A). Under 45 deg illumination, the blue ventral eye reflects a narrow-band short wavelength spectrum (~445 nm peak), whereas the green dorsal region produces a higher intensity, broad-band longer wavelength reflectance (470–600 nm flat peak). Fig. 6 demonstrates how reflectance changes across the eye of individual *Pu th1* while holding the illumination angle at 45 deg and rotating the eye in 15 deg steps from ventral to dorsal.

In situ spectral analysis of larval eyeshine

The analysis of eyeshine spectra in the natural environment was performed using radiometric data collected concurrently with each *in situ* photographic series (see '*In situ* spectral analysis' in Materials and methods). The spectral properties of eyeshine were analysed *in situ* from two individuals representing different species and eyeshine reflectances: *Pullosquilla thomassini* and *Pseudosquillana richeri*. Since *P. thomassini* displays different reflectance spectra across the retina (Fig. 6), we included both a dorsal and ventral reflectance measurement in our spectral analysis. To examine further whether

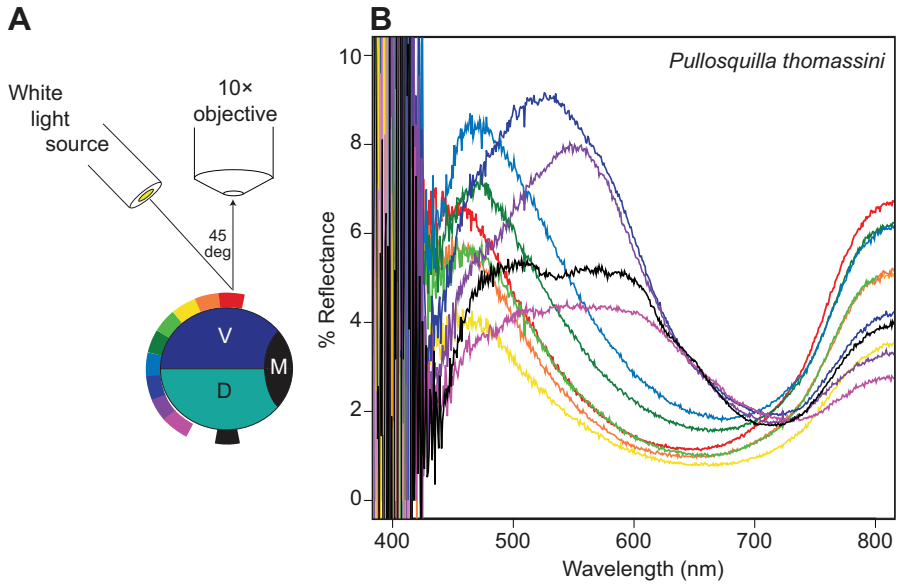

Fig. 6. *Pullosquilla thomassini* eyeshine reflectance across the eye. (A) Diagram depicting locations of reflectance spectral measurements collected in 15 deg step rotations under 45 deg illumination of a single eye. V, ventral eye region; D, dorsal eye region; M, medial edge of eye. (B) Reflectance spectra changes in both wavelength reflectance and intensity across the eye. The color of each spectrum represents the location of each measurement on the eye, depicted by the colored bars on the lateral edge of the eye in A. The low levels of short-wavelength light available from the light source combined with the relatively weak reflectance of the eye (due to eye area) is responsible for the noise observed in the spectral plot below 410 nm.

P. thomassini and *P. richeri* eyeshine spectra are adaptive, we calculated what the eyeshine of a non-endemic species, *Squilla empusa* from the Western Atlantic Ocean, would produce if it were in the Lizard Island light environment by multiplying the *S. empusa* eyeshine reflectance by Lizard Island irradiance spectra. *Squilla empusa* larval eyeshine reflectance data were collected using the same methods as *G. falcatus* during an independent field study at the Duke University Marine Laboratory (Beaufort, North Carolina, USA; July 2010).

Normalized, raw eyeshine reflectances from *P. thomassini* and *P. richeri* are presented in Fig. 7A. When multiplied by the irradiance spectrum measured during each photographic series, calculated eyeshine demonstrates a close match between its wavelength of peak reflection and the radiance spectra of the background light environment. These results are consistent regardless of sun position, time of day, or depth (Fig. 7B–E) for both of the Lizard Island-occurring species. It should be noted that while the blue, ventral eyeshine of *P. thomassini* may not seem to be well matched in shallow, broad-spectrum water, the green dorsal eyeshine is well matched to the background radiance at this depth (Fig. 7C). By comparison, the calculated reflectance spectrum from larval eyes of *S. empusa* demonstrates a poor match to background radiances for most Lizard Island spectral environments (Fig. 8A,B,D). The long-wavelength shifted, broad spectral reflectance of *S. empusa* only appears to provide an adequate match to the peak wavelengths measured at shallow depths (1 m), where the environmental spectrum is much broader (Fig. 8C).

DISCUSSION

General

By systematically testing animals in their natural light environments, we demonstrated that stomatopod larval eyeshine effectively reduces retinal contrast and is spectrally matched to the viewing background at depth. Matches between spectra of background radiances and calculated eyeshine from endemic species suggest that spectral matching is adaptive to particular habitats (Figs 7, 8). Although, one might suspect that any eyeshine reflector could match the environmental radiance, we found that *Squilla empusa* eyeshine reflectance estimates are poorly matched to the Lizard Island light environment (Fig. 8). *Squilla empusa* eyeshine reflectance is likely matched to the long-wavelength shifted radiance of its native light environment in the Western Atlantic Ocean, though the radiometric data necessary to test this are unavailable. Regardless, data from Lizard Island stomatopod larvae present the first documented example of a pelagic reflective camouflage spectrally matched to the viewing background.

In general, eyeshine performs like other pelagic mirror reflectors, as predicted by theoretical models of crypsis (Johnsen and Sosik, 2003). Eyeshine produces significantly less contrast with the background environment than a dark object control from all examined viewing angles, solar azimuths and solar elevations, depths, and rotations (Figs 3, 4). Additionally, the reduction of eyeshine reflectivity in dead larvae produces a significant increase in the contrast of the eye when compared to the eyeshine contrast of a living animal (Fig. 4B). These data strongly support the hypothesis that eyeshine serves as a camouflage for the opaque retina in stomatopod larval eyes.

Though all eyeshine measurements of Michelson contrast were close to 0.0, the value of no contrast, there was variation in the range of contrast values among data sets. The maximum range of contrast values within a single photographic series was −0.28 to +0.22 (*Pu th1*, 11 m depth), while the minimum range of contrast values only varied from −0.16 to −0.03 (*Pu th4*, depth 17 m; Fig. 4). For datasets where a single animal was photographed in two different illumination conditions (*Pu th1* and *Pu th2*), the animal demonstrated a significant change in the ranges of contrast values measured between the two conditions (*Pu th1*, P=0.0025; *Pu th2*, P=4.51e^{-7}). Changes in contrast did not vary significantly with the rotation of the animal or viewing angle, leading to the conclusion that eyeshine contrast is influenced by the illumination conditions (such as depth and solar elevation) rather than the physical light-reflecting properties of the reflector.

Though solar elevation and depth were the only illumination factors within our dataset to affect eyeshine contrast, we could not reconcile the two factors from one another. The individuals photographed in two different series in June 2012 (*Pu th1* and *Pu th2*) were each photographed at different depths and solar elevations. Given these data, the influence of each variable could not be ascertained. We revisited this experiment in March 2014 and successfully imaged an individual (*Pu th6*) at different solar elevations, controlling for depth, and found no significant change in the variation of eye contrast. While these results may suggest that

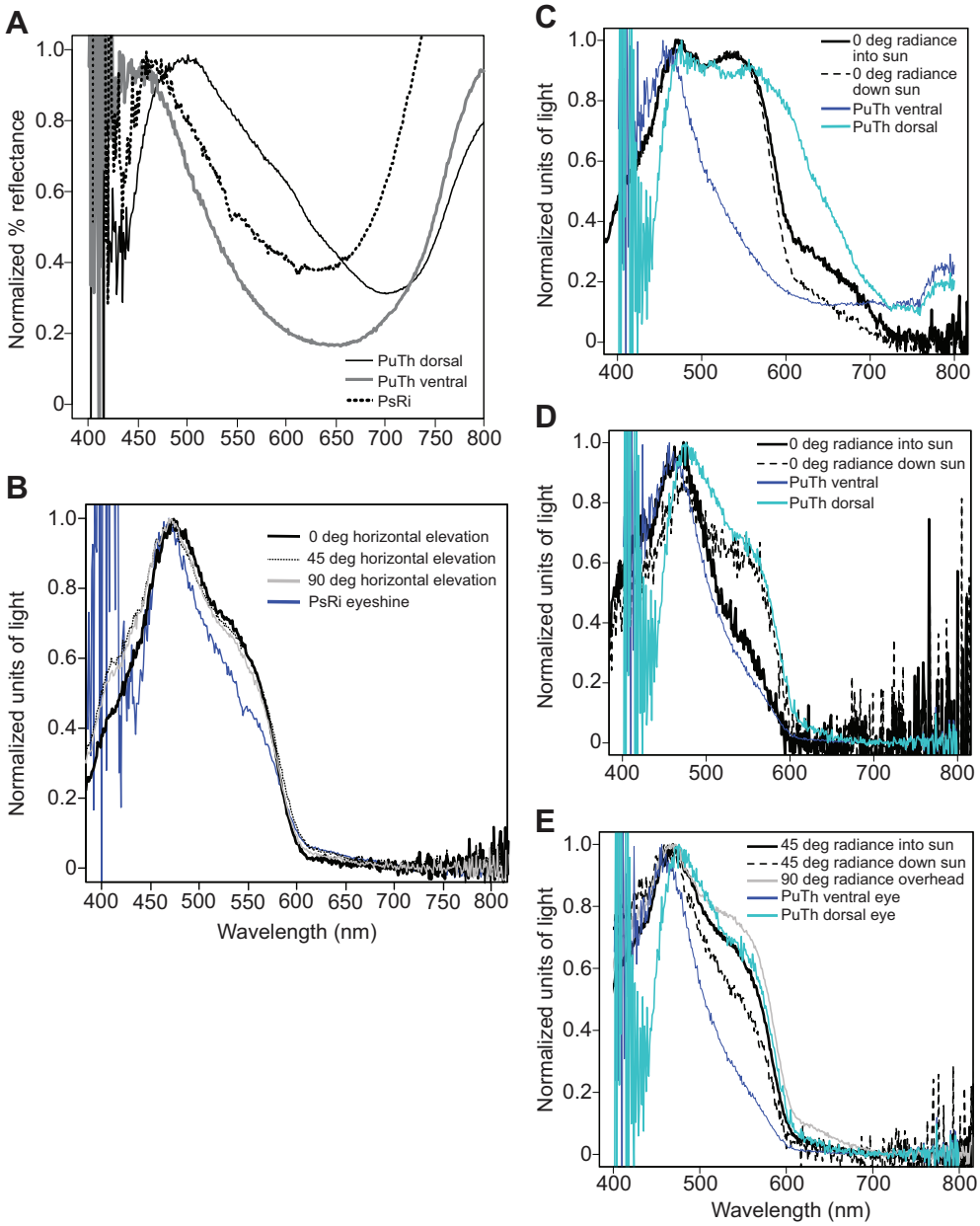

Fig. 7. Calculated eyeshine spectra in natural lighting conditions. Noise observed below 410 nm in eyeshine reflectances is due to low levels of short-wavelength light available from the light source combined with the relatively weak reflectance of the eye (due to eye area). (A) *Pullosquilla thomassini* (PuTh) and *Pseudosquillana richeri* (PsRi) larval eyeshine reflectance curves. Reflectance curves from both the ventral and dorsal regions of PuTh eyes were used in our analyses. (B−E) Calculated eyeshine reflectances versus selected radiances of different viewing angles above the horizon. All black and gray curves represent background radiances; blue traces represent calculated eyeshine reflectance. (B) *P. richeri* at 6 m depth versus 0, 45 and 90 deg viewing angle radiances collected from Down sun solar azimuth. (C) *P. thomassini* calculated eyeshine at 1 m depth versus 0 deg viewing angle radiance. (D) *P. thomassini* calculated eyeshine at 11 m depth versus 0 deg viewing angle radiance. (E) *P. thomassini* calculated eyeshine at 11 m depth versus 45 and 90 deg viewing angle radiances. Radiance solar azimuths for C−E are indicated in the keys.

depth is a primary influence in eye contrast variation, it is difficult to interpret without further analysis. Future experiments that control for depth and solar elevation are necessary for resolving the influence on eye contrast with the background. Due to our small sample size, our observations of changes to eye contrast with solar elevation and depth may also be an artifact of individual variation, which cannot be resolved without further studies. Regardless, the evidence suggests that overall eyeshine is an effective mechanism of reducing contrast in any natural illumination conditions.

Ecological significance

Predation is a strong selective force that may drive the evolution of stomatopod larval eyeshine. Previous work demonstrates that rates of fish predation on transparent cladocerans increase when the size and pigmentation of the eyespot is increased via dietary uptake of India ink (Zaret, 1972). Though predation is a likely force driving the evolution of stomatopod larval eyeshine evolution, this hypothesis remains untested. Future behavioral experiments analogous to those with transparent cladocerans will provide an interesting test of the relationship between eyeshine contrast and predation rates. Such experiments, however, would not address whether the range of contrast values observed from stomatopod larval eyes are detectable by predators. To determine if eyeshine contrast is ecologically significant in its worst illumination conditions (most contrast), the lower threshold limits of contrast detection for a predator must be determined through sensitivity modeling experiments.

Stomatopod larvae perform diel vertical migrations, whereby they are found at depth during the day and rise to the surface at night to feed (Ohtomi et al., 2005). Our findings that most eyeshine spectra are well matched to light environments at deeper depths agrees with this aspect of stomatopod larval ecology, since larvae are expected to be found away from the surface at depth during the day. Poor matching between larval eyeshine and broad-spectrum environmental radiance at shallow, 1 m daytime depths may be of little consequence in nature, since larvae would rarely occur in such a habitat. Evidence of spectral matching between shallow (1 m) radiances and the dorsal green eyeshine in *P. thomassini*, however, suggests that this species

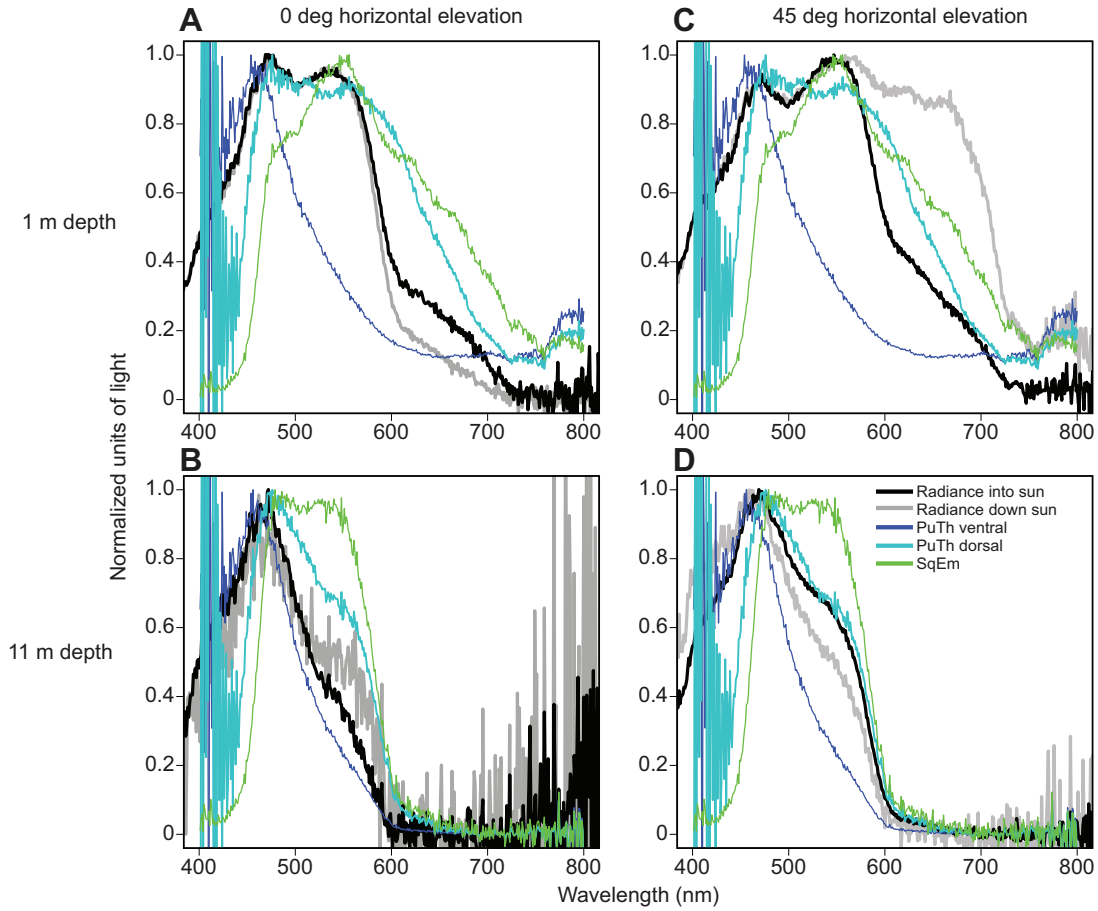

Fig. 8. Calculated eyeshine reflectance from *Pullosquilla thomassini* and *Squilla empusa* larvae versus radiance measurements at different depths, solar azimuths and viewing angles above the horizon. Depth and viewing direction are as follows: (A) 1 m, 0 deg horizontal elevation; (B) 11 m, 0 deg horizontal elevation; (C) 1 m, 45 deg horizontal elevation; and (D) 11 m, 45 deg horizontal elevation. Black and gray traces represent measured background radiances; green (*S. empusa*) and blue traces (*P. thomasini*) represent calculated reflectance from eyeshine for the indicated environment.

may be camouflaging at shallower depths per an aspect of their behavioral ecology that remains to be characterized.

The unusual blue and green regionalized eyeshine seen in *P. thomassini* larval eyes suggests some interesting hypotheses regarding its function in this particular species. It is possible that the two spectrally different regions of the eye (green, dorsal hemisphere and blue, ventral hemisphere) are a mechanism for counter-shading. The green region of eyeshine shows better spectral matching against shallow, background radiances, suggesting that it may be adaptive for camouflage in a shallower habitat. Until more is known regarding the daytime behavior and location of *P. thomassini* larvae, we cannot evaluate the functional significance of this regionalized eyeshine. However, given that the blue-ventral, green-dorsal eyeshine of *P. thomassini* is present throughout the entire range of larval stages (authors' personal observations in early and last stages), we can assume this novel structure plays a specific role in the ecology and is not related to developmental changes to the eye. Studies that target the swimming posture of *P. thomassini* larvae and the diel vertical migration range of this species may help to identify the particular evolutionary pressures that led to such a novel eyeshine solution.

Eyeshine-producing structures

The structures responsible for producing stomatopod larval eyeshine are not currently understood, though photonic structures are widely used for camouflage in the aquatic environment. Broad-band reflectors, or silvery mirrors, are a common and effective solution to camouflaging in the pelagic environment (Johnsen and Sosik, 2003). The size of the object being camouflaged may provide insight as to why stomatopod larvae do not use a silver reflector to hide their opaque retina. Though the stalked eyes on a larval stomatopod seem prominent, they are in fact quite small by comparison with the flanks of a silvery fish, which are understood to produce broad-band reflection via multiple layers of guanine crystals with varying quarter-wavelength thicknesses (Denton and Land, 1971). The space required for a typical silver reflector is perhaps not available in a stomatopod eye, which is only ~500 μm in maximum diameter (Denton and Land, 1971); therefore, eyeshine must either be produced by a simple quarter-wavelength multilayer reflector or by a relatively thin coherent scattering photonic structure. The terrestrial diamond weevil, *Entimus imperialis*, has been shown to use spectrally matched reflections from diamond-type photonic crystals for camouflage in forested environments (Wilts et al., 2012). While it is unlikely this specific type of photonic structure is found in stomatopod larval eyes, a comparable large-domain-type photonic crystal may be responsible for producing such finely tuned reflectance spectra.

Existing evidence suggests that eyeshine-producing structures may be composed of three-dimensionally arranged vesicles. Transmission electron microscopic images of eye structures in

caridean shrimp (*Palaemonetes*) larvae, which possess a greenish-gold reflecting eyeshine, show layers of tightly packed, spherical vesicles at the junction of the optics and the photoreceptor layer – the hypothesized location of crustacean eyeshine-producing structures (Douglass, 1986; Douglass and Forward, 1989). Some species of adult Squilloid and Lysiosquilloid stomatopods also possess green light-reflecting pigments on the outer margin of the retina (Marshall et al., 1991). As with the *Palaemonetes* larvae, these structures are composed of spherical vesicles, indicative of an amorphous solid with short-range order. We hypothesize that similar structures may exist in the eyes of stomatopod larvae. Investigations into the ultrastructure that is the source of stomatopod larval eyeshine are currently underway.

Our diverse taxonomic sampling suggests that eyeshine is widespread within Stomatopoda as a mechanism of larval ocular camouflage. Though eyeshine has been observed in all examined stomatopod larval species, it is unclear as to whether the mechanism used to produce eyeshine is identical across species, since different eyeshine reflectance spectra exist. Future investigations that characterize the photonic structures responsible for producing eyeshine should include a diverse taxonomic sampling of species so as to examine how these novel light-reflecting structures vary among stomatopods.

MATERIALS AND METHODS

Animal collection

The majority of larvae were captured in June 2012 at Lizard Island Research Station (Queensland, Australia), with a smaller subset of samples collected at the same location in March 2014. All collections were performed at night either while wading or scuba diving. During night dives at depths of 6–18 m we took advantage of the innate, positive phototactic behavior of early pelagic stage stomatopod larvae (Dingle, 1969) and attracted larvae to an underwater light source (Underwater Kinetics AquaSun eLED; Poway, CA, USA). Larvae were collected in gallon-size, resealable bags and later sorted in the laboratory. All deep-water collection periods began within 30 min of sunset and had a maximum duration of 40 min. Collections in shallow water (~1 m depth) were routinely performed while wading near shore between 20:00 and 22:00 h. Animals were captured using hand-held dip nets and the same light source was used during collections at depth. Larvae were maintained individually in plastic cups in the laboratory at ambient temperatures (~26°C) in seawater without food. All experiments were conducted within 48 h of capture. Larvae were identified *post hoc* via DNA barcoding at the University of Maryland, Baltimore County (Baltimore, MD, USA) (see Feller et al., 2013).

In situ imaging

Live-mounted animals were photographed in their natural environment (*in situ*) using a Canon G12 camera (Lake Success, New York, NY, USA) and a calibrated rotational chuck mounted on a tripod. Prior to imaging, we established that the spectral properties of larval eyeshine change with illumination angle. Consequently, we tested eyespot contrast from a variety of viewing angles and directions that best represented the upper hemisphere of view for an observer positioned under water (Fig. 2). We imaged targets from a fixed, benthic position that provided views of the animal from below. Each selected viewing angle and larval posture can be broken down into four components: solar azimuth, viewing angle above the horizon, larval long axis orientation, and larval rotational angle (Fig. 2). The four solar directions included: into the sun's azimuth ('Into sun', 0 deg), right of the sun ('Right sun', 90 deg), away from the sun ('Down sun', 180 deg), and left of the sun ('Left sun', 270 deg). In each direction relative to the sun, the animal was viewed at three viewing angles relative to the horizon (0, 45 and 90 deg) while the long axis of the animal was held either vertically (V) or horizontally (H). As the 90 deg viewing angle position produces redundancy between H and V animals (e.g. [Into sun, 90, H] is the same as [Right sun, 90, V]) only H images were collected for all 90 deg views relative to the horizon. To further view eyeshine reflectance at various orientations, at each position the animal was rotated in four 90 deg turns so as to image eyeshine from the ventral, left, dorsal and right aspects (Fig. 2, inset photographs). In each series, a total of 80 unique views of each animal were thus produced from the described components.

The changes in lighting conditions that accompanied the viewing angles and directions of our images necessitated the use of the camera's automatic shutter speed selection. Using a fixed F-stop of 8, the automatic camera generated three successive exposures for every raw format image captured: the automatically selected exposure, an underexposed image one stop below, and an overexposed image one stop above the automatic exposure. Thus a final total of 240 images per series was collected for image contrast analysis.

As a control, a small, black-painted spherical object was used as an opaque dark standard. This 1-mm diameter standard was included in each photographic measurement, placed within a centimeter of the larval target. After photographing, each animal was fixed in absolute ethanol for DNA barcoding and identified *post hoc* per the methods described in Feller et al. (Feller et al., 2013). Specimens were considered positively identified if the genetic distance relative to a reference sequence of the cytochrome oxidase I (COI) gene was ≤3% (Barber and Boyce, 2006). The only unknown larval specimen in this study was tentatively assigned to the genus *Harpiosquilla* because the smallest sequence distance to a COI gene reference (10%) was to that of *Harpiosquilla harpax*. Since no morphological or molecular barcode record of any adult *Harpiosquilla* species presently exists at Lizard Island, it is likely that this larva represents an undescribed squilloid species from this region. Alternatively, the individual could represent a larva that is passing through from a distant location on a local current. Until DNA barcodes are documented for a greater selection of stomatopod species, the true identity of this individual will remain unclear.

All barcode sequences of the cytochrome oxidase subunit I mitochondrial gene were deposited in GenBank (GB-KJ828804, KJ828805, KJ828806, KJ828807, KJ828808, KJ828809, KJ828810, KJ828811). Since eyeshine often disappears when a larva dies, only animals that survived to the fixation procedure were used for the experimental analysis. We utilized the reduction in eyeshine post mortem as a second control by including a dead larva in the *Pu th6* photographic series (March 2014). Both the dead larva (which died prior to experimentation) and a dark standard were mounted within a centimeter of the living specimen. Two photographic series at different solar elevations were collected using the dead eye control.

Image analysis

Before analysing the *in situ* images, we calibrated the digital camera for its brightness sensitivity across the 8-bit dynamic range of each red (R), green (G) or blue (B) pixel. To do so, we photographed a series of six gray standards (white, gray 8, gray 6.5, gray 5, gray 3.5 and black; Macbeth Colorchecker; Baltimore, MD, USA) illuminated under diffuse, natural sunlight. In Adobe Photoshop, both the average green and blue channel pixel values were measured from each gray standard in each exposure in the series. This produced values between 0 and 255, the maximum range for any 8-bit pixel channel. For every exposure, five error ratios were calculated between neighboring gray standards and plotted versus pixel value to determine how pixel value changes with exposure using our camera system. A linear regression of this plot was then calculated from both the blue and green channel measurements and used to produce the following correction formula:

$$y = \frac{x}{-0.0004x + 0.8}. \quad (1)$$

Using this formula, a corrected pixel value (y) of each experimental image could be calculated for each raw 8-bit measurement (x) from a photograph. Calibration measurements from the blue and green channels produced the same correction formula. Due to the attenuation of different wavelengths of light under water with depth, only the blue and green 8-bit channels provide reliable data for the range of depths measured in these experiments. Measurements from either of these channels were sufficient for our analysis since there was no difference in the correction formula. Because green wavelengths attenuate at a slightly faster rate than blue, we selected the

green 8-bit channel for our analysis so as to minimize potential saturation of pixel values at shallow depths.

For analysis of experimental images, a 15 deg circular template was centered on the mounted larva in each raw format image using Adobe Photoshop. The corrected average green channel pixel value within this circle was taken to be the background radiance. Near-field objects, such as the larval mount or reef substrate, were excluded from this measurement by selecting the averaged area of scattered pelagic light within the circle using a drawing tablet (Wacom Intuos; Vancouver, WA, USA). The 15 deg region was selected to duplicate the acceptance angle of the probe used for radiometric data collection (see '*In situ* spectral analysis' below). Eye radiance was determined by averaging all pixels within the larval retina. The same procedure was performed for radiance measurements of the dark standard. Photographs in which the retina was not in focus were not included in the final analysis.

Contrast is a quantitative measurement of how bright or dark an object is relative to a given background and can be measured using either the Michelson or the Weber formula for contrast (Johnsen, 2012). When addressing questions of inherent contrast of an object at a fixed distance, as was the case with this study, either Michelson or Weber contrast formulae may be used (Johnsen, 2012). Weber contrast is often preferred to calculate attenuation of contrast with distance of small objects (Johnsen, 2012) or for sensitivity modeling of animals viewing eyeshine (O'Carroll and Wiederman, 2014). Since our objective was not designed to model the visibility of larval eyes to hypothetical viewers, but rather to test the inherent contrast of stomatopod larval eyes with the background environment, we chose to calculate the Michelson contrast (C_M) of our subject with the background:

$$C_M = \frac{\left(L_{eye} - L_{background}\right)}{\left(L_{eye} + L_{background}\right)}, \quad (2)$$

where L_{eye} is the eye radiance and $L_{background}$ is the background radiance. In this way, we were better able to analyse inherent contrast, since the values produced from this formula range between −1 and 1, with the value of no contrast equal to zero.

To examine changes in eyeshine contrast with time of day, or solar elevation, the refracted solar elevation at the time of each photographic series was calculated using Snell's law:

$$\theta_2 = \sin^{-1}\left(\frac{n_1 \sin\theta_1}{n_2}\right). \quad (3)$$

Snell's law describes the angle light is refracted as it enters a medium with a different refractive index (n). For our calculations, we used the n of air (n_1=1.0) and the n of water (n_2=1.33). Solar elevation data (θ_S) were acquired from the NOAA Solar Position Calculator (www.esrl.noaa.gov/gmd/grad/solcalc/; accessed 21 April 2014) for the specific date and time of each photographic series at the Lizard Island co-ordinates (−14.673°S, 145.454°E). θ_S was then used to determine θ_1, the angle subtended by the sun and the zenith (θ_1=90 deg − θ_S). The refracted solar elevation of the sun (θ_{RS}) was determined by subtracting θ_2 from 90 deg. These calculations provide the position of the sun within Snell's window, the 96 deg cone through which light in the air is refracted and compressed above an underwater viewer (Lythgoe, 1979; Johnsen, 2012).

Statistical analyses

All statistical analyses were performed in R. Each data set was tested for normal distribution using a Shapiro–Wilk normality test. All data sets were normally distributed. To test for differences between contrast data measured from animal eyeshine and the dark standards, a Wilcoxon rank sum test (also known as a Mann–Whitney *U*-test) was performed. Alternatively, a Wilcoxon signed rank test was used to test for differences between eyeshine contrast data sets measured from a single individual at different depths and/or times of day. A Bonferroni correction method was employed during multiple comparisons of specific data. In our analyses, specific data sets were compared two to three times, thus the significance threshold (α) for a given analysis was either 0.025 or 0.017. All statistical results, as well as corrected significance thresholds, are summarized in Table 1.

In situ spectral analysis

Environmental spectra were measured during each photographic series using a calibrated underwater spectrometer, Subspec (Andor Technology/Oriel, Brisbane, Queensland). At the beginning of each series a cosine corrector (CC-3, Ocean Optics, Dunedin, FL, USA) was attached to a 40 cm long by 100 μm diameter optical fiber (UV-Vis; Ocean Optics) to collect downwelling irradiance. Radiance for all angles at which photographs were taken was measured using a 15 deg acceptance angle probe.

Prior to underwater photography, larvae were glued to sticks and affixed to a calibrated angle mount, which was suspended under water and imaged via a submerged 10× microscope objective (Leitz Dialux 22; Wetzlar, Germany) (Fig. 5A). The front face of the 10× objective was protected from seawater by wrapping it in a plastic film. Larvae were illuminated by a white-light, LS-1 tungsten halogen lamp (Ocean Optics) connected to a 1 μm optical fiber (UV-Vis; Ocean Optics). The optical fiber was submerged and fixed on the calibrated angle mount to illuminate the specimen at one of four fixed angles relative to the optical axis of the 10× objective: 90, 75, 60 or 45 deg. Physical interference between the light source and the objective prevented reflectance measurements from illumination angles smaller than 45 deg. Light was guided to a spectrometer (QE65000; Ocean Optics) using a 1-μm diameter optical fiber (UV-Vis; Ocean Optics) and a custom probe-microscope adaptor attached to the epi-eyepiece of the microscope (in place of the actual eyepiece; Fig. 5A). Reflectance measurements were collected using SpectraSuite software (Ocean Optics) operated on a MacBook Pro (Apple; Cupertino, CA, USA). A measurement of 100% reflectance was obtained at the beginning of each data collection session using a Spectralon diffuse white standard (Labsphere; North Sutton, NH, USA). Due to the ultraviolet opacity of the microscope system, wavelengths less than 400 nm were not included in our analyses. A linear polarizer was rotated to 0 and 90 deg in the path of reflected light to measure the degree of polarized light reflected from the retina. All measurements were acquired from live specimens.

To calculate the eyeshine reflectance spectra in the natural environment, the eye reflectance spectrum from a 45 deg illumination angle (the illumination angle from which maximum reflectance was determined, Fig. 5C,D) measured for each individual was multiplied by the downwelling irradiance measured for an *in situ* condition of interest. Computed eyeshine was compared to radiance spectra collected from all viewing directions for a given *in situ* condition. Since radiance was collected in tandem with the photographic series, this provided real-time environmental spectra present during each image capture. Due to different values of intensities among irradiance, radiance and reflectance spectral data, all spectra were normalized to their maxima for comparison. Using these same methods, we also computed the eyeshine reflectance from larvae of *Squilla empusa*, a Western Atlantic stomatopod species, in the Lizard Island light environment to test whether eyeshine from a species inhabiting a different light environment (such as the Western Atlantic ocean) can provide an adequate spectral match to any background, or if instead it is adaptive to specific environments.

Acknowledgements
The authors are grateful to Dr Megan Porter (University of South Dakota) for assistance with Subspec measurements; John Cataldi (University of Maryland, Baltimore County) for construction of custom experimental apparatuses; Julian Partridge (University of Bristol) for spectral analyses; Lizard Island Research Station staff for technical and logistical support in the field; as well as Dr Sönke Johnsen (Duke University), Dr Nicholas Roberts (University of Bristol) and Dr N. Justin Marshall (University of Queensland) for their expert counsel on various aspects of this project.

Competing interests
The authors declare no competing financial interests.

Author contributions
The initial concept for this study was proposed by T.W.C. All further designs, methods and analyses were performed by K.D.F. under the mentorship of T.W.C. The manuscript was composed in its entirety by K.D.F., with revisions by T.W.C.

Funding
This work was supported by a grant from the United States Air Force Office of Scientific Research (FA9550-12-1-0321).

References

Barber, P. and Boyce, S. L. (2006). Estimating diversity of Indo-Pacific coral reef stomatopods through DNA barcoding of stomatopod larvae. *Proc. Biol. Sci.* **273**, 2053-2061.

Breder, C. M. (1962). On the significance of transparency in Osteichthid fish eggs and larvae. *Copeia* **1962**, 561-567.

Chiou, T. H., Mäthger, L. M., Hanlon, R. T. and Cronin, T. W. (2007). Spectral and spatial properties of polarized light reflections from the arms of squid (*Loligo pealeii*) and cuttlefish (*Sepia officinalis* L.). *J. Exp. Biol.* **210**, 3624-3635.

Clarke, W. D. (1963). Function of bioluminescence in mesopelagic organisms. *Nature* **198**, 1244-1246.

Cronin, T. and Jinks, R. (2001). Ontogeny of vision in marine crustaceans. *Am. Zool.* **41**, 1098-1107.

Cronin, T. W., Marshall, N. J., Caldwell, R. and Pales, D. (1995). Compound eyes and ocular pigments of crustacean larvae (Stomatopoda and Decapoda, Brachyura). *Mar. Freshwat. Behav. Physiol.* **26**, 219-231.

Denton, E. J. and Land, M. F. (1971). Mechanism of reflexion in silvery layers of fish and cephalopods. *Proc. R. Soc. B* **178**, 43-61.

Denton, E. J., Gilpin-Brown, J. B. and Wright, P. G. (1972). The angular distribution of the light produced by some mesopelagic fish in relation to their camouflage. *Proc. R. Soc. B* **182**, 145-158.

Dingle, H. (1969). Ontogenetic changes in phototaxis and thigmokinesis in stomatopod larvae. *Crustaceana* **16**, 108-110.

Douglas, J. M., Cronin, T. W., Chiou, T. H. and Dominy, N. J. (2007). Light habitats and the role of polarized iridescence in the sensory ecology of neotropical nymphalid butterflies (Lepidoptera: Nymphalidae). *J. Exp. Biol.* **210**, 788-799.

Douglass, J. K. (1986). *The Ontogeny of Light and Dark Adaptation in the Compound Eyes of Grass Shrimp, Palaemonetes Pugio.* PhD dissertation, Duke University, Durham, NC, USA. Accessed from author.

Douglass, J. and Forward, R. (1989). The ontogeny of facultative superposition optics in a shrimp eye: hatching through metamorphosis. *Cell Tissue Res.* **258**, 289-300.

Feller, K. D., Cronin, T. W., Ahyong, S. T. and Porter, M. L. (2013). Morphological and molecular description of the late-stage larvae of Alima Leach, 1817 (Crustacea: Stomatopoda) from Lizard Island, Australia. *Zootaxa* **3722**, 22-32.

Harzsch, S., Miller, J., Benton, J., Dawirs, R. R. and Beltz, B. (1998). Neurogenesis in the thoracic neuromeres of two crustaceans with different types of metamorphic development. *J. Exp. Biol.* **201**, 2465-2479.

Harzsch, S., Benton, J., Dawirs, R. R. and Beltz, B. (1999). A new look at embryonic development of the visual system in decapod crustaceans: neuropil formation, neurogenesis, and apoptotic cell death. *J. Neurobiol.* **39**, 294-306.

Johnsen, S. (2001). Hidden in plain sight: the ecology and physiology of organismal transparency. *Biol. Bull.* **201**, 301-318.

Johnsen, S. (2012). *The Optics of Life: A Biologist's Guide to Light in Nature*. Princeton, NJ: Princeton University Press.

Johnsen, S. (2014). Hide and seek in the open sea: pelagic camouflage and visual countermeasures. *Ann. Rev. Mar. Sci.* **6**, 369-392.

Johnsen, S. and Sosik, H. M. (2003). Cryptic coloration and mirrored sides as camouflage strategies in near-surface pelagic habitats: implications for foraging and predator avoidance. *Limnol. Oceanogr.* **48**, 1277-1288.

Johnsen, S., Widder, E. A. and Mobley, C. D. (2004). Propagation and perception of bioluminescence: factors affecting counterillumination as a cryptic strategy. *Biol. Bull.* **207**, 1-16.

Jutte, P. A., Cronin, T. W. and Caldwell, R. L. (1998). Photoreception in the planktonic larvae of two species of pullosquilla, a lysiosquilloid stomatopod crustacean. *J. Exp. Biol.* **201**, 2481-2487.

Loew, E. R. (1976). Light, and photoreceptor degeneration in the Norway lobster, *Nephrops norvegicus* (L.). *Proc. R. Soc. B* **193**, 31-44.

Lythgoe, J. N. (1979). *The Ecology of Vision*. Oxford: Clarendon Press.

McFall-Ngai, M. (1990). Crypsis in the pelagic environment. *Am. Zool.* **30**, 175-188.

Marshall, N., Land, M., King, C. and Cronin, T. (1991). The compound eyes of mantis shrimps (Crustacea, Hoplocarida, Stomatopoda). II. Colour pigments in the eyes of stomatopod crustaceans: Polychromatic vision by serial and lateral filtering. *Philos. Trans. R. Soc. B* **334**, 57-84.

Nilsson, D. E. (1983). Evolutionary links between apposition and superposition optics in crustacean eyes. *Nature* **302**, 818-821.

Nilsson, D.-E. (1995). Eye design, vision and invisibility in planktonic invertebrates. In *Zooplankton: Sensory Ecology and Physiology* (ed. P. H. Lenz, D. K. Hartline, J. E. Purcell and D. L. Macmillan), pp.149-162. Amsterdam: Gordon and Breach.

Nilsson, D. E. and Nilsson, H. L. (1983). Eye camouflage in the isopod crustacean *Astacilla longicornis* (Sowerby). *J. Mar. Biol. Ecol.* **68**, 105-110.

O'Carroll, D. C. and Wiederman, S. D. (2014). Contrast sensitivity and the detection of moving patterns and features. *Philos. Trans. R. Soc. B* **369**, 20130043.

Ohtomi, J., Kawazoe, H. and Furota, T. (2005). Larval stage composition and morphological change during larval development of the Japanese mantis shrimp, *Oratosquilla oratoria* (De Haan, 1844) (Stomatopoda, Squillidae) in Tokyo Bay, Japan. *Crustaceana* **78**, 1325-1337.

Stavenga, D. G., Giraldo, M. A. and Leertouwer, H. L. (2010). Butterfly wing colors: glass scales of *Graphium sarpedon* cause polarized iridescence and enhance blue/green pigment coloration of the wing membrane. *J. Exp. Biol.* **213**, 1731-1739.

Stavenga, D. G., Wilts, B. D., Leertouwer, H. L. and Hariyama, T. (2011). Polarized iridescence of the multilayered elytra of the Japanese jewel beetle, *Chrysochroa fulgidissima*. *Philos. Trans. R. Soc. B* **366**, 709-723.

Williams, B., Greenwood, J. and Jillett, J. (1985). Seasonality and duration of the developmental stages of *Heterosquilla tricarinata* (Claus, 1871) (Crustacea: Stomatopoda) and the replacement of the larval eye at metamorphosis. *Bull. Mar. Sci.* **36**, 104-114.

Wilts, B. D., Michielsen, K., Kuipers, J., De Raedt, H. and Stavenga, D. G. (2012). Brilliant camouflage: photonic crystals in the diamond weevil, *Entimus imperialis*. *Proc. Biol. Sci.* **279**, 2524-2530.

Zaret, T. M. (1972). Predators, invisible prey, and the nature of polymorphism in the Cladocera (Class Crustacea). *Limnol. Oceanogr.* **17**, 171-184.